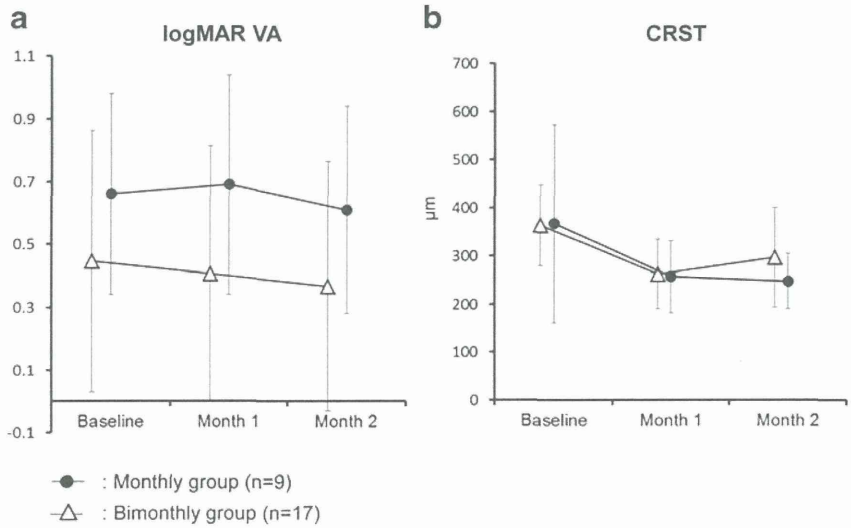

Fig. 5 Clinical outcomes of two groups. The *solid circles* indicate the monthly injection group; the *open triangles* indicate the bimonthly injection group. **a** The logMAR BCVA levels in the two groups. There are no significant differences between baseline and months 1 or 2. **b** The CRST measurements in the two groups. In the bimonthly injection group, there are significant ($P<0.001$) differences between baseline and months 1 and 2. In the monthly injection group, the CRST is significantly ($P<0.05$) different at month 1 compared with baseline

significant decrease of VEGF level seen at month 2 is interesting, because in rabbits and monkeys treated with one IVR injection the half-life of intraocular ranibizumab was about 3 days. From these studies, the period for ranibizumab to inhibit intraocular VEGF activity in patients with AMD was expected to last up to 30 days [28, 29]. However, Krohne and colleagues confirmed that the aqueous half-life of 0.5 mg IVR injections in human nonvitrectomized eyes with AMD, diabetic retinopathy, and retinal vein occlusion was a mean of 7.19 days [30], much longer than in animals. That finding was consistent with the present results in vivo.

Incomplete suppression of VEGF at month 2 in bimonthly group may indicate that the ranibizumab dose may be insufficient to suppress aqueous VEGF for 2 whole months, and the aqueous VEGF level may begin to increase at a certain time point between 1 month and 2 months. Our result showed that one intrealvireal injection of ranibizumab may suppress VEGF for an extended time, which was more than 1 month but less than 2 months in human eyes with AMD.

In the bimonthly injection group, there were three eyes of three patients whose aqueous VEGF level didn't change significantly 2 months after the first injection ($P=0.23$). One patient's VEGF concentration increased from 101.01 pg/ml to 161.95 pg/ml 2 months after first injection. This may result from the fact that this patient seemed to be a non-responder to ranibizumab treatment, because the CRST of the patient did not decrease (217 μm at baseline, 217 μm 1 month after the first injection and 216 μm 2 months after the first injection) and the logMAR VA did not improve after rainibizumab injection either (0.82 at baseline, 1.0 one month after the first injection and 1.0 two months after the first injection). The other two patients' aqueous VEGF levels were slightly increased after the first injection. This may be due to variability of VEGF concentration in aqueous humor; their VEGF

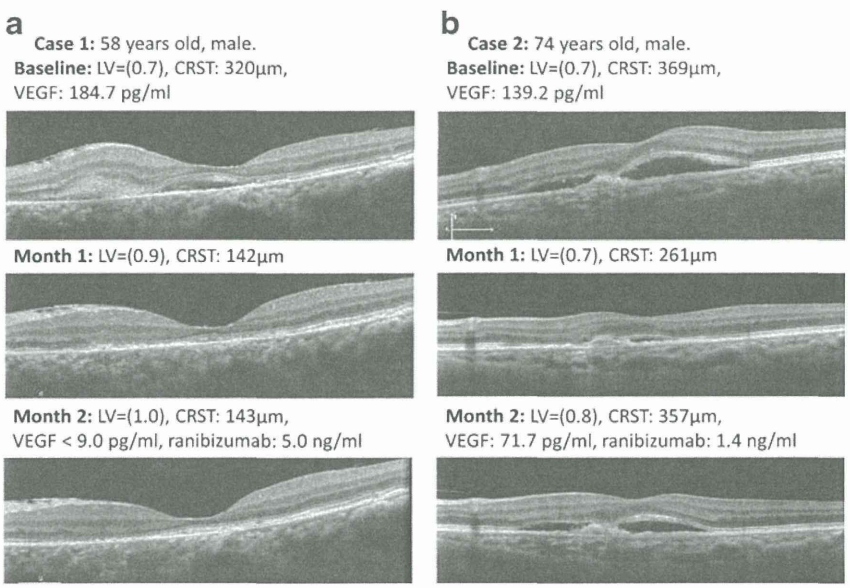

Fig. 6 Findings on OCT in eyes treated with bimonthly injections at baseline and months 1 and 2. **a** The OCT images obtained from a patient whose aqueous VEGF concentration at month 2 has decreased to less than the lowest detectable limit. **b** The OCT images obtained from a patient whose aqueous VEGF concentration at month 2 is higher than the lowest detectable limit. LV=left visual acuity

baseline levels (41.85 pg/ml and 42.73 pg/ml) were much lower than in other patients, which may be the reason for the small change in VEGF level after ranibizumab injection.

The aqueous ranibizumab level in the monthly injection group was higher than that at month 2 in the bimonthly injection group after the initial injection. This is justifiable because of drug metabolism and excretion. The present study was the first to describe aqueous ranibizumab concentrations in human eyes with AMD 2 months after IVR injections. Surprisingly, in the current study the ranibizumab was detectable at month 2 in eyes treated with bimonthly injections. According to our observations, the VEGF concentration decreased with increases in the aqueous ranibizumab concentration. The current measurements indicated that an aqueous concentration of about 5 ng/ml or greater of ranibizumab suppressed the aqueous VEGF level under the lowest threshold. We deduced that 5 ng/ml or greater is the lowest effective dose of ranibizumab that can suppress the VEGF level below threshold. In a primate model, the ranibizumab concentration in the vitreous was 2- to 3.3-fold higher than in the aqueous [29]. Furthermore, the half maximal inhibitory concentration of ranibizumab for reducing VEGF was estimated to be 11 to 27 ng/ml [31]. Therefore, the lowest ranibizumab concentration of 5 ng/ml that can completely suppress the VEGF activity in the aqueous in the current study can be estimated to be 10 to 16.5 ng/ml in the vitreous, which was consistent with a previous report [31].

Interestingly, when the aqueous VEGF level was below the lowest detectable limit in most eyes, the CRST was maintained through the second month (Fig. 6a). In contrast, when the aqueous VEGF level was higher than the lowest detectable limit, the CRST decreased at month 1 but recurrent thickening was seen at month 2 (Fig. 6b). Therefore, the VEGF level may indicate the changes in the CRST after IVR treatment in eyes with AMD. Although in Fig. 6b the CRST at month 2 increased compared with month 1, it was still lower than baseline, which also indicates the benefit of bimonthly injections.

In the current study, although there was no significant difference in the VA results at months 1 and 2 compared with baseline in the two groups, the VA improvement was clinically relevant. In the bimonthly injection group, the mean VA improved by 5.5 letters, and in the monthly injection group, the mean VA improved by 2.5 letters at month 2, while a significant improvement in the CRST occurred in the eyes in the monthly injection group at month 1 and the eyes in the bimonthly injection group at months 1 and 2. This may have occurred because the changes in the CRST preceded the changes in the BCVA [32, 33]. The 2-month follow-up in the current study may have been too short for significant BCVA improvements in a small number of eyes.

The current study should be considered a pilot study with a small number of eyes and a short observation period. From our study, although bimonthly IVR injections would not ensure complete VEGF inhibition in all patients, it not only provides morphologic but also functional benefits to patients with AMD. In eyes with AMD, morphologic recurrences (increased central retinal thickness) occurred at an average of 93.7 days and functional recurrence (decreased VA) occurred at an average of 114.3 days [33], both of which are much longer than 2 months. Based on this, the injection interval of 60 days is enough to prevent significant recurrences.

Compared with monthly injections, the number of bimonthly intravitreal injections administered during 1 year was six, fewer than 12 monthly injections, and the bimonthly injection regimen eases the patients' treatment burden economically and psychologically. Based on the positive results of the CLEAR-IT 2 study, the VIEW I and the VIEW 2 study compared the efficacy and safety of monthly and bimonthly injections of aflibercept with ranibizumab injections, the gold standard, and both studies reported noninferiority in visual outcomes and safety at 1 year [25, 34]. Although the outcomes of the VIEW 1 and VIEW 2 studies showed that aflibercept with 8-week dosing was not inferior to monthly IVR injections of ranibizumab over a 1-year period, according to the current findings, another study with more patients and a longer follow-up period is warranted to evaluate the efficacy of bimonthly injections of ranibizumab for treating AMD.

In conclusion, in this pilot study with limited follow-up, intravitreal injection of ranibizumab can suppress aqueous VEGF completely for 1 month in most cases. Its effect does not last sufficiently for 2 months to suppress VEGF completely in most cases, although aqueous VEGF at 2 months after intravitreal injection of ranibizumab is less than that before injection in most cases.

Acknowledgments Supported in part by a grant from the Ministry of Education, Culture, Sports, Science and Technology of Japan (#24592668) and a grant from the Ministry of Health, Labour and Welfare.

The authors have no proprietary interest in any aspect of this study. The funding organizations had no role in the design or conduct of this study.

References

1. Aiello LP, Pierce EA, Foley ED, Takagi H, Chen H, Riddle L, Ferrara N, King GL, Smith LE (1995) Suppression of retinal neovascularization in vivo by inhibition of vascular endothelial growth factor (VEGF) using soluble VEGF-receptor chimeric proteins. Proc Natl Acad Sci U S A 92:10457–10461
2. Lopez PF, Sippy BD, Lambert HM, Thach AB, Hinton DR (1996) Transdifferentiated retinal pigment epithelial cells are immunoreactive for vascular endothelial growth factor in surgically excised age-related macular degeneration-related choroidal neovascular membranes. Invest Ophthalmol Vis Sci 37:855–868
3. Frank RN, Amin RH, Eliott D, Puklin JE, Abrams GW (1996) Basic fibroblast growth factor and vascular endothelial growth factor are present in epiretinal and choroidal neovascular membranes. Am J Ophthalmol 122:393–403

4. Kvanta A, Algvere PV, Berglin L, Seregard S (1996) Subfoveal fibrovascular membranes in age-related macular degeneration express vascular endothelial growth factor. Invest Ophthalmol Vis Sci 37:1929–1934
5. Kliffen M, Sharma HS, Mooy CM, Kerkvliet S, de Jong PT (1997) Increased expression of angiogenic growth factors in age-related maculopathy. Br J Ophthalmol 81:154–162
6. Krzystolik MG, Afshari MA, Adamis AP, Gaudreault J, Gragoudas ES, Michaud NA, Li W, Connolly E, O'Neill CA, Miller JW (2002) Prevention of experimental choroidal neovascularization with intravitreal anti-vascular endothelial growth factor antibody fragment. Arch Ophthalmol 120:338–346
7. Witmer AN, Vrensen GF, Van Noorden CJ, Schlingemann RO (2003) Vascular endothelial growth factors and angiogenesis in eye disease. Prog Retin Eye Res 22:1–29
8. Klaver CC, Wolfs RC, Vingerling JR, Hofman A, de Jong PT (1998) Age-specific prevalence and causes of blindness and visual impairment in an older population: the Rotterdam Study. Arch Ophthalmol 116:653–658
9. Bressler NM (2004) Age-related macular degeneration is the leading cause of blindness. JAMA 291:1900–1901
10. Friedman DS, O'Colmain BJ, Muñoz B, Tomany SC, McCarty C, de Jong PT, Nemesure B, Mitchell P, Kempen J, Eye Diseases Prevalence Research Group (2004) Prevalence of age-related macular degeneration in the United States. Arch Ophthalmol 122:564–572
11. Resnikoff S, Pascolini D, Etya'ale D, Kocur I, Pararajasegaram R, Pokharel GP, Mariotti SP (2004) Global data on visual impairment in the year 2002. Bull World Health Organ 82:844–851
12. Tong JP, Chan WM, Liu DT, Lai TY, Choy KW, Pang CP, Lam DS (2006) Aqueous humor levels of vascular endothelial growth factor in polypoidal choroidal vasculopathy and choroidal neovascularization. Am J Ophthalmol 141:456–462
13. Jonas JB, Neumaier M (2007) Vascular endothelial growth factor and basic fibroblast growth factor in exudative age-related macular degeneration and diffuse diabetic macular edema. Ophthalmic Res 39:139–142
14. Ahn JK, Moon HJ (2009) Changes in aqueous vascular endothelial growth factor and pigment epithelium-derived factor after ranibizumab alone or combined with verteporfin for exudative age-related macular degeneration. Am J Ophthalmol 148:718–724
15. Funk M, Karl D, Georgopoulos M, Benesch T, Sacu S, Polak K, Zlabinger GJ, Schmidt-Erfurth U (2009) Neovascular age-related macular degeneration: intraocular cytokines and growth factors and the influence of therapy with ranibizumab. Ophthalmology 116: 2393–2399
16. Sawada O, Miyake T, Kakinoki M, Sawada T, Kawamura H, Ohji M (2010) Aqueous vascular endothelial growth factor after intravitreal injection of pegaptanib or ranibizumab in patients with age-related macular degeneration. Retina 30:1034–1038
17. Rosenfeld PJ, Brown DM, Heier JS, Boyer DS, Kaiser PK, Chung CY, Kim RY, MARINA Study Group (2006) Ranibizumab for neovascular age-related macular degeneration. N Engl J Med 355:1419–1431
18. Brown DM, Kaiser PK, Michels M, Soubrane G, Heier JS, Kim RY, Sy JP, Schneider S, ANCHOR Study Group (2006) Ranibizumab versus verteporfin for neovascular age-related macular degeneration. N Engl J Med 355:1432–1444
19. Mitchell P, Korobelnik JF, Lanzetta P, Holz FG, Prünte C, Schmidt-Erfurth U, Tano Y, Wolf S (2010) Ranibizumab (Lucentis) in neovascular age-related macular degeneration: evidence from clinical trials. Br J Ophthalmol 94:2–13
20. Regillo CD, Brown DM, Abraham P, Yue H, Ianchulev T, Schneider S, Shams N (2008) Randomized, double-masked, sham-controlled trial of ranibizumab for neovascular age-related macular degeneration: PIER Study year 1. Am J Ophthalmol 145:239–248
21. Abraham P, Yue H, Wilson L (2010) Randomized, double-masked, sham-controlled trial of ranibizumab for neovascular age-related macular degeneration PIER study year 2. Am J Ophthalmol 150: 315–324
22. Schmidt-Erfurth U, Eldem B, Guymer R, Korobelnik JF, Schlingemann RO, Axer-Siegel R, Wiedemann P, Simader C, Gekkieva M, Weichselberger A, EXCITE Study Group (2011) Efficacy and safety of monthly versus quarterly ranibizumab treatment in neovascular age-related macular degeneration: the EXCITE study. Ophthalmology 118:831–839
23. Holash J, Davis S, Papadopoulos N, Croll SD, Ho L, Russell M, Boland P, Leidich R, Hylton D, Burova E, Ioffe E, Huang T, Radziejewski C, Bailey K, Fandl JP, Daly T, Wiegand SJ, Yancopoulos GD, Rudge JS (2002) VEGF-Trap: A VEGF blocker with potent antitumor effects. Proc Natl Acad Sci U S A 99: 11393–11398
24. US Food and Drug Administration (2011) FDA labeling information — Eylea http://www.accessdata.fda.gov/drugsatfda_docs/label/2011/125387lbl.pdf. Accessed Nov 2011
25. Heier JS, Brown DM, Chong V, Korobelnik JF, Kaiser PK, Nguyen QD, Kirchhof B, Ho A, Ogura Y, Yancopoulos GD, Stahl N, Vitti R, Berliner AJ, Soo Y, Anderesi M, Groetzbach G, Sommerauer B, Sandbrink R, Simader C, Schmidt-Erfurth U, VIEW 1 and VIEW 2 Study Groups (2012) Intravitreal aflibercept (VEGF Trap-Eye) in wet age-related macular degeneration. Ophthalmology 119:2537–2548
26. Verteporfin Roundtable Participants (2005) Guidelines for using verteporfin (Visudyne) in photodynamic therapy for choroidal neovascularization due to age-related macular degeneration and other causes: update. Retina 25:119–134
27. Funatsu H, Yamashita H, Noma H, Mimura T, Nakamura S, Sakata K, Hori S (2005) Aqueous humor levels of cytokines are related to vitreous levels and progression of diabetic retinopathy in diabetic patients. Graefes Arch Clin Exp Ophthalmol 243:3–8
28. Bakri SJ, Shyder MR, Reid JM, Pulido JS, Ezzat MK, Singh RJ (2007) Pharmacokinetics of intravitreal ranibizumab (Lucentis). Ophthalmology 114:2179–2182
29. Gaudreault J, Fei D, Rusit J, Suboc P, Shiu V (2005) Preclinical pharmacokinetics of ranibizumab (rhufabv2) after a single intravitreal administration. Invest Ophthalmol Vis Sci 46:726–733
30. Krohne TU, Liu Z, Holz FG, Meyer CH (2012) Intraocular pharmacokinetics of ranibizumab following a single intravitreal injection in humans. Am J Ophthalmol 154:682–686
31. Lucentis (ranibizumab injection). Highlights of prescribing information. Available at: http://www.gene.com/gene/products/information/pdf/lucentis-prescribing.pdf. Accessed April 15, 2011.
32. Hoerster R, Muether PS, Hermann MM, Koch K, Kirchhof B, Fauser S (2011) Subjective and functional deterioration in recurrences of neovascular AMD are often preceded by morphologic changes in optic coherence tomography. Br J Ophthalmol 95:1424–1426
33. Muether PS, Hermann MM, Viebahn U, Kirchhof B, Fauser S (2012) Vascular endothelial growth factor in patients with exudative age-related macular degeneration treated with ranibizumab. Ophthalmology 119:2082–2086
34. Heier JS, Boyer D, Nguyen QD, Marcus D, Roth DB, Yancopoulos G, Stahl N, Ingerman A, Vitti R, Berliner AJ, Yang K, Brown DM, CLEAR-IT 2 Investigators (2011) CLEAR-IT 2 Investigators. The 1-year results of CLEAR-IT 2, a phase 2 study of vascular endothelial growth trap-eye dosed as-needed after 12-week fixed dosing. Ophthalmology 118:1098–1106

Clinical Ophthalmology

Dovepress

open access to scientific and medical research

Open Access Full Text Article

CASE SERIES

Adaptive optics fundus images of cone photoreceptors in the macula of patients with retinitis pigmentosa

Naoki Tojo
Tomoko Nakamura
Chiharu Fuchizawa
Toshihiko Oiwake
Atsushi Hayashi

Department of Ophthalmology, Graduate School of Medicine and Pharmaceutical Sciences, University of Toyama, Toyama, Japan

Background: The purpose of this study was to examine cone photoreceptors in the macula of patients with retinitis pigmentosa using an adaptive optics fundus camera and to investigate any correlations between cone photoreceptor density and findings on optical coherence tomography and fundus autofluorescence.

Methods: We examined two patients with typical retinitis pigmentosa who underwent ophthalmological examination, including measurement of visual acuity, and gathering of electroretinographic, optical coherence tomographic, fundus autofluorescent, and adaptive optics fundus images. The cone photoreceptors in the adaptive optics images of the two patients with retinitis pigmentosa and five healthy subjects were analyzed.

Results: An abnormal parafoveal ring of high-density fundus autofluorescence was observed in the macula in both patients. The border of the ring corresponded to the border of the external limiting membrane and the inner segment and outer segment line in the optical coherence tomographic images. Cone photoreceptors at the abnormal parafoveal ring were blurred and decreased in the adaptive optics images. The blurred area corresponded to the abnormal parafoveal ring in the fundus autofluorescence images. Cone densities were low at the blurred areas and at the nasal and temporal retina along a line from the fovea compared with those of healthy controls. The results for cone spacing and Voronoi domains in the macula corresponded with those for the cone densities.

Conclusion: Cone densities were heavily decreased in the macula, especially at the parafoveal ring on high-density fundus autofluorescence in both patients with retinitis pigmentosa. Adaptive optics images enabled us to observe in vivo changes in the cone photoreceptors of patients with retinitis pigmentosa, which corresponded to changes in the optical coherence tomographic and fundus autofluorescence images.

Keywords: adaptive optics fundus camera, cone photoreceptor, fundus autofluorescence, optical coherence tomography, retinitis pigmentosa

Introduction

Retinal degenerations constitute a group of inherited diseases that result in progressive loss of photoreceptors. In retinitis pigmentosa, cone dysfunction is secondary to rod degeneration and ultimately results in loss of fine visual acuity.[1,2] Survival of photoreceptors seems to be closely correlated with visual functioning in patients with retinitis pigmentosa.[2,3] Therefore, assessment of photoreceptors may be very important in evaluation of disease progression in patients with the disease.

The functioning of the retinal pigment epithelium can be visualized by fundus autofluorescence using a short wave length, which reflects lipofuscin accumulation in the retinal pigment epithelium or disrupted phagocytosis.[4] Indeed, other studies have

Correspondence: Atsushi Hayashi
Department of Ophthalmology, Graduate School of Medicine and Pharmaceutical Sciences, University of Toyama, 2630 Sugitani, Toyama, 930-0194, Japan
Tel +81 76 434 7363
Fax +81 76 434 5037
Email ganka@med.u-toyama.ac.jp

submit your manuscript | www.dovepress.com
Dovepress
http://dx.doi.org/10.2147/OPTH.S39879

reported that an abnormal fundus autofluorescence ring is present in more than half of patients with retinitis pigmentosa examined, and that the length of the inner and outer segment (IS/OS) line determined by optical coherence tomography (OCT) is significantly correlated with the diameter of the fundus autofluorescence ring.[2,5,6] In a study using new retinal imaging devices, such as spectral-domain OCT and adaptive optics scanning laser ophthalmoscopy, it was shown that patients with retinitis pigmentosa had abnormal cone spacing values, which were correlated with reduction in visual acuity and the amplitudes of multifocal electroretinograms.[7]

In the present study, we analyzed cone photoreceptors in the macula of patients with retinitis pigmentosa using an adaptive optics fundus camera, and examined the relationship between cone photoreceptor density and abnormal findings on fundus autofluorescence and OCT images.

Materials and methods

We examined two patients with retinitis pigmentosa at Toyama University Hospital. Each patient underwent a complete eye examination, including measurement of decimal best-corrected visual acuity and collection of scotopic and photopic full-field electroretinographic, OCT, fundus autofluorescent, and adaptive optics fundus camera images. OCT was performed using a three-dimensional OCT-2000 system (Topcon Corp, Tokyo, Japan). Electroretinography was performed using an LE-4000 system (Tomey Corp, Aichi, Japan) according to the International Society for Clinical Electrophysiology of Vision standards. Fundus autofluorescent images were obtained with a scanning laser ophthalmoscope (F-10, Nidek Co, Aichi, Japan). A blue laser light (490 nm) was used for excitation and a wide band-pass filter with a cutoff at 521 nm was inserted in front of the detector for fundus autofluorescence. Adaptive optics fundus images were taken with a rtx-1™ flood-illuminated adaptive optics fundus camera (Imagine Eyes, Orsey, France). The rtx-1 has a resolution of 1.6 μm with a 4 × 4 degree imaging field of view and an illumination wavelength of 850 nm. The adaptive optics images taken with the rtx-1 were analyzed using the original cone analysis software created by the manufacturer.

To establish a healthy control group for purposes of comparison with the patients suffering from retinitis pigmentosa, we also included five healthy control eyes from five subjects. Adaptive optics images of the healthy control eyes were taken using the rtx-1 and analyzed with the same software. All procedures conformed to the tenets of the Declaration of Helsinki. The study protocol for the adaptive optics fundus camera was approved by the institutional review board of the University of Toyama. All subjects gave their written informed consent before participation in the study.

Results

Case 1

Case 1 was a 31-year-old woman with best-corrected visual acuity of 0.9 in the right eye and 1.0 in the left eye. A color fundus photograph of the right eye showed fundus changes typical of retinitis pigmentosa, ie, black bone spicule pigmentation and depigmentation, narrowing of the retinal vessels, and retinal degeneration (Figure 1A). Scotopic and photopic full-field electroretinograms were undetectable in both eyes (data not shown). An abnormal parafoveal ring of high-density fundus autofluorescence was observed in the fundus autofluorescence image (arrows in Figure 1B), which indicated abnormal phagocytosis and concomitant lipofuscin accumulation in the retinal pigment epithelium. The fovea showed a normal dark area on fundus autofluorescence.

The OCT image of the macula of the right eye (Figure 1C) showed an irregular cone outer segment tips line and IS/OS line at the fovea. The normal dark macular fundus autofluorescence area corresponded to the area with the residual cone outer segment tips line and IS/OS line (Figure 1C and D).

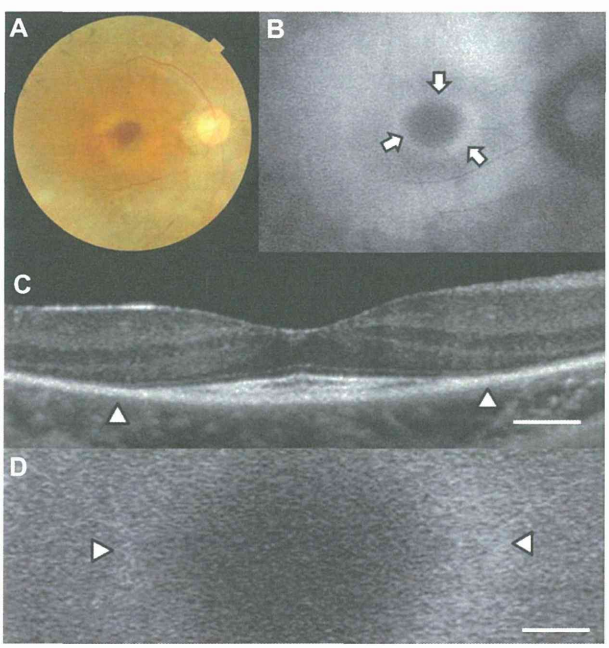

Figure 1 Fundus images of the right eye in case 1. Color fundus photograph (**A**), short-wave length fundus autofluorescence photograph (**B**), spectral-domain optical coherence tomographic image (**C**), and magnified fundus autofluorescence photograph of the macula (**D**). Arrows show a parafoveal high-density fundus autofluorescence ring (**B**). Arrowheads show the border of the external limiting membrane and the inner segment and outer segment line (**C**) and parafoveal high-density fundus autofluorescence ring (**D**). Bar = 200 μm (**C** and **D**).

The high-density autofluorescent ring in the fundus autofluorescence image corresponded to the border of the IS/OS line and the external limiting membrane in the OCT image (arrowheads in Figure 1C and D). However, it was difficult to determine whether the inner or outer border of the high-density fundus autofluorescence ring corresponded to the termination of the IS/OS line and external limiting membrane in the OCT image.

Figure 2A shows a panoramic image of cone photoreceptors in a 2.42 × 3.16 mm area including the fovea of the right eye taken with the adaptive optics fundus camera. The number of cone photoreceptors was reduced in this panoramic adaptive optics image. A ring-shaped area with blurred cone mosaics and some patchy dark areas around the fovea was observed (arrows in Figure 2A). This ring-shaped blurred area corresponded to the high-density autofluorescent ring by fundus autofluorescence. Cone photoreceptors in the adaptive optics images were analyzed using the manufacturer's software. The cone density panorama map obtained from the image in Figure 2A is shown in Figure 2B. The blurred ring in Figure 2A shows a reduced density of cone photoreceptors (arrows in Figure 2B). In the region outside of the ring, areas of higher cone densities resembling islands were observed (arrowheads in Figure 2B). Adaptive optics fundus photographs were taken several times and photographs that were blurred by motion artifacts were not used.

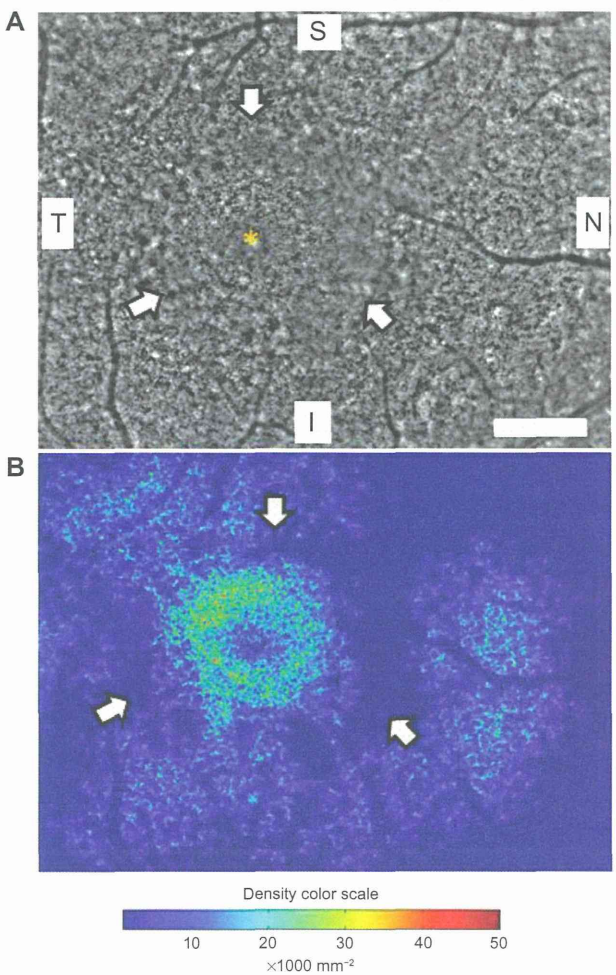

Figure 2 Panoramic adaptive optics fundus image (**A**) and cone density map (**B**) of the right eye in case 1. (**A**) Panoramic adaptive optics fundus image 2.42 × 3.16 mm in area including the fovea (yellow asterisk). Arrows show a blurred ring area of cone mosaics which corresponds to the parafoveal high-density fundus autofluorescence ring. Bar = 200 μm (**A**). (**B**) Panoramic cone density map of the same area as in (**A**).
Notes: Arrows show a ring of low density area which corresponds to the blurred area in the adaptive optics image. Arrowheads show focal high density areas of cone photoreceptors. The color scale of the density is shown.
Abbreviations: S, superior; I, inferior; N, nasal; T, temporal.

Four 200 × 200 μm areas at the nasal or temporal retina were selected (avoiding large retinal vessels) and analyzed using the software (Figure 3). The nasal or temporal areas were selected at the blurred ring (N600 and T600) and outside of the ring (N1300 and T1100). The N600 and T600 distances were 600 μm from the foveal center, and the N1300 and T1100 distances were 1300 μm and 1100 μm from the foveal center. The results for the three types of cone analyses at the four areas are shown in Figure 3, and the data are shown in Table 1. The results of the cone analyses for the five healthy control eyes in the same four areas as examined in case 1 are also shown in Table 1. The control data are expressed as the mean ± standard deviation for the five healthy control eyes. Figure 4 shows panoramic (6.22 × 0.96 mm) and 0.2 × 0.2 mm adaptive optics images in one of the five healthy control eyes obtained by rtx-1.

The densities of cone photoreceptors were lower at all four areas than those of the healthy control eyes (Table 1). As shown in Figure 2B, the cone densities at the blurred area of the ring (T600 and N600) were lower than the areas outside of the ring (T1100 and N1300), even though the OCT image showed loss of the IS/OS line and external limiting membrane. The results for the spacing and Voronoi domains were correlated with those of the densities.

Case 2

Case 2 was a 56-year-old woman with best-corrected visual acuity of 1.2 in both eyes. A color fundus photograph of the right eye showed fundus characteristics typical of retinitis pigmentosa, as also seen in case 1 (Figure 5A). Scotopic and photopic full-field electroretinograms were undetectable in both eyes (data not shown). A parafoveal ring with a high density of autofluorescence was observed by fundus autofluorescence (arrows in Figure 5B), but only the inner border of the temporal part of the ring was demarcated (arrowhead in Figure 5B). The IS/OS line and the external

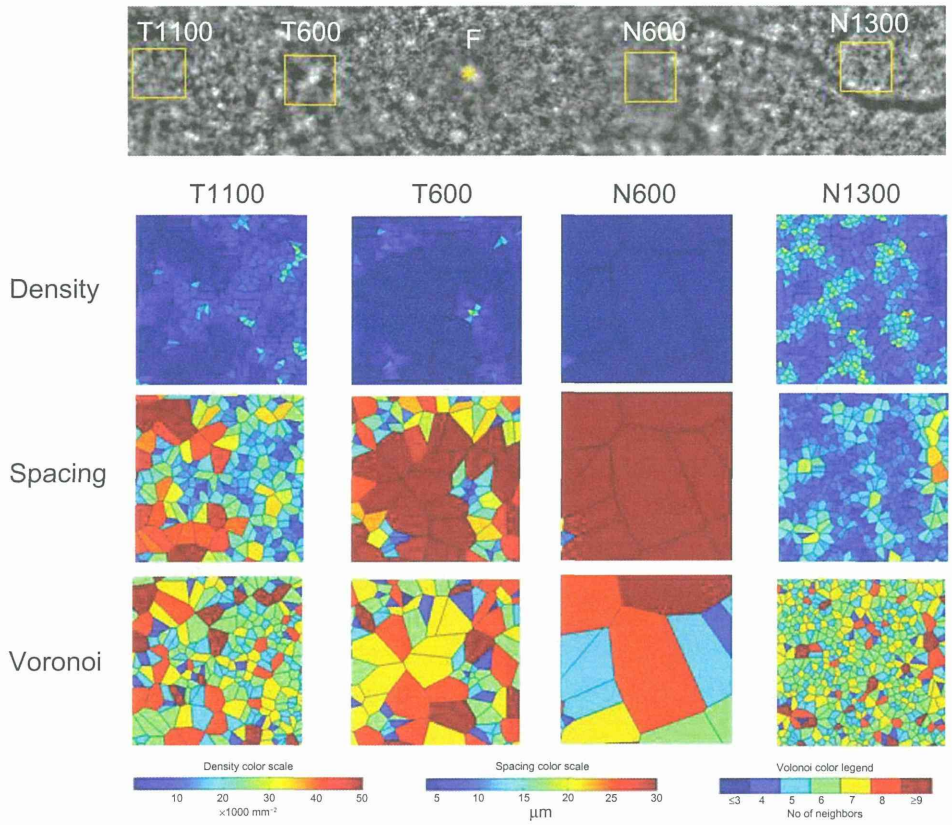

Figure 3 Cone analyses of the parafoveal areas in case 1.
Notes: Four areas of 0.2 × 0.2 mm were selected for the nasal or temporal regions at the blurred ring (N600 and T600), and outside of the ring (N1300 and T1100). The N600, T600, N1300, and T1100 distances were 600 μm, 600 μm, 1300 μm, and 1100 μm from the foveal center, respectively. Cone analysis maps of the density, spacing, and Voronoi domains are shown with color scales for each of the four areas.

limiting membrane were better preserved than in case 1, and the border of the IS/OS line and the external limiting membrane was observed in the OCT image (arrowheads in Figure 6A). The nasal part of the high-density parafoveal fundus autofluorescence ring corresponded to the border of the IS/OS line and the external limiting membrane (arrowheads in Figure 6B), but the temporal part of the ring was not clear. Figure 6C shows a panoramic image of cone photoreceptors in a 1.05 × 5.88 mm area including the fovea of the right eye. The cone photoreceptors of the adaptive optics image were reduced in the macula, and the area with blurred cone mosaics and patchy dark spots corresponded to only the nasal part of the parafoveal ring (arrowheads in Figure 6C). The cone photoreceptors in the adaptive optics images were analyzed using the manufacturer's software. The cone density panoramic map (Figure 6D) shows that the area of the blurred cone mosaics in the nasal part of the ring has reduced cone densities (arrowheads in Figure 6D).

Four 200 × 200 μm areas at the nasal or temporal retina (Figure 7) were selected (avoiding large retinal vessels) and

Table 1 Results of cone analyses at four areas in the macula of the right eye in case 1 and healthy control eyes

	T1100	T600	N600	N1300
Density (/mm^2)				
Case 1	5409	2053	124	12381
Healthy control (n = 5)	18118 ± 1961	24691 ± 2411	22822 ± 3322	15260 ± 1851
Spacing (μm)				
Case 1	14.22	20.66	62.67	9.85
Healthy control (n = 5)	8.23 ± 0.44	7.04 ± 034	7.34 ± 0.53	8.95 ± 0.51
Voronoi (% of six-sided polygons)				
Case 1	31.9	22.0	0	36.3
Healthy control (n = 5)	51.6 ± 5.0	46.6 ± 4.0	44.0 ± 5.1	46.0 ± 4.2

Note: Data for healthy controls are shown as the mean ± standard deviation.

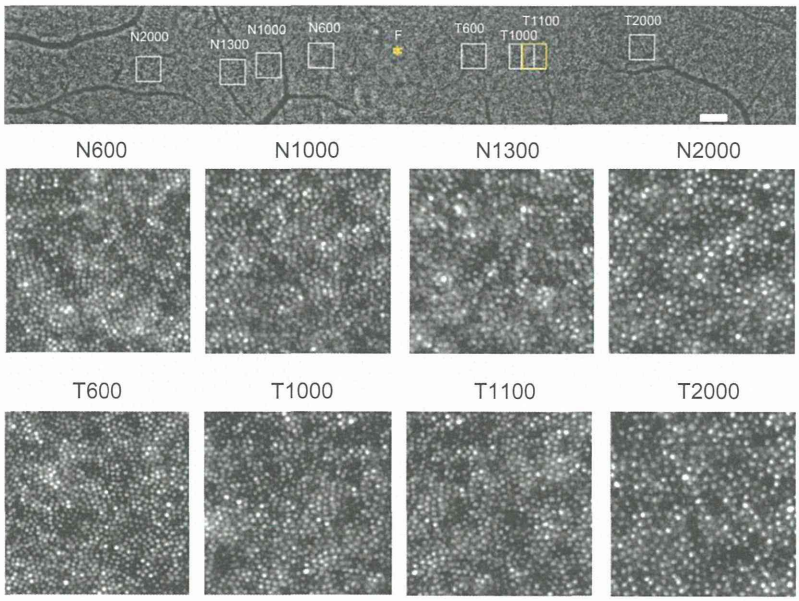

Figure 4 Panoramic and focal adaptive optics images of the macular area in one eye for the healthy controls.
Notes: A panoramic adaptive optics image showing a 6.22 × 0.96 mm area including the foveal center (yellow asterisk, F). Bar = 200 μm. Eight 0.2 × 0.2 mm areas were selected at the nasal or temporal retina and each adaptive optics image is shown. The N600, N1000, N1300, N2000, T600, T1000, T1100, and T2000 distances were 600 μm, 1000 μm, 1300 μm, 2000 μm, 600 μm, 1000 μm, 1100 μm, and 2000 μm from the foveal center, respectively.

analyzed using the manufacturer's software. The nasal area was selected at the inside of the blurred ring (N1000) and at the border of the ring (N2000). The temporal areas (T1000 and T2000) were selected at the same distance as the two nasal areas. The N1000 and T1000 distances were 1000 μm from the foveal center, and those of N2000 and T2000 were 2000 μm from the foveal center. The results for the three types of cone analyses at the four areas are shown in Figure 7, and the data are shown in Table 2. The mean densities of the cone photoreceptors were lower at T1000, N1000, and N2000 than for the healthy controls (Table 2). Because the temporal part of the fundus autofluorescence ring was not clear, the number of cone photoreceptors remained the same as that in the healthy controls at T2000 in case 2. The results for the spacing and Voronoi domains were correlated with those of the densities.

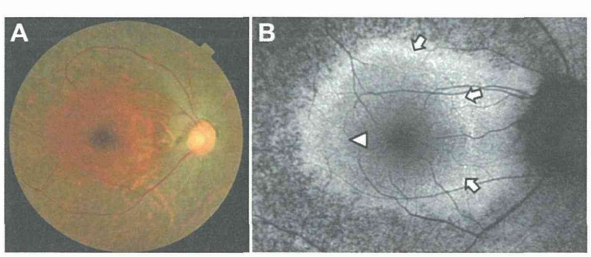

Figure 5 Color fundus photograph (**A**) and short-wavelength fundus autofluorescence photograph (**B**) of the right eye in case 2. Arrows show an incomplete parafoveal ring of high-density fundus autofluorescence (**B**). The arrowhead shows the inner border of the high-density fundus autofluorescence ring (**B**).

Discussion

Retinitis pigmentosa causes progressive degeneration of photoreceptors and the retinal pigment epithelium. These changes were observed as an abnormal parafoveal ring of high-density or low-density fundus autofluorescence at

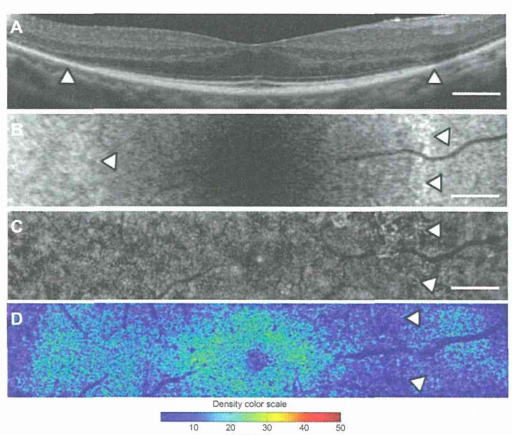

Figure 6 Macular images of OCT (**A**), fundus autofluorescence (**B**), adaptive optics (**C**), and the panoramic cone density map (**D**) of the right eye in case 2. The OCT image shows the border of the inner segment and outer segment line and the external limiting membrane at the arrowheads (**A**). Magnified fundus autofluorescence image of the macula shows part of the high-density fundus autofluorescence ring at the nasal retina [arrowheads in (**B**)]. The temporal inner border of the ring is indicated by an arrowhead (**B**). The adaptive optics panoramic image of a 5.9 × 1.1 mm area appears as a blurred region with some dark patchy areas at the nasal side of the high-density fundus autofluorescence ring (arrowheads in **C**). A panoramic cone density map of the same area as in (**C**) shows low densities at the nasal ring [arrowheads in (**D**)]. Bar = 200 μm (**A**–**C**).
Note: The color scale of the density is shown.
Abbreviation: OCT, optical coherence tomography.

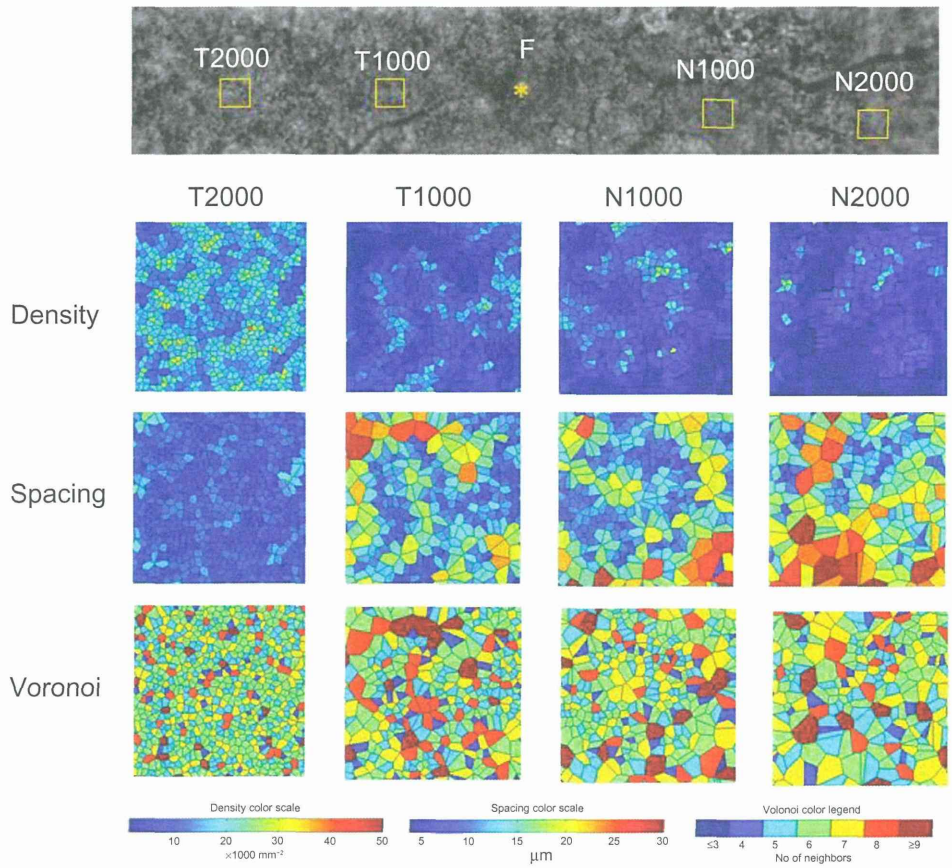

Figure 7 Cone analyses of the parafoveal areas in case 2.
Notes: Four areas were selected at the nasal areas inside of the blurred ring (N1000) and at the ring (N2000) and the temporal areas at the same distance from the two nasal areas (T1000 and T2000). The N1000, T1000, N2000, and T2000 distances were 1000 μm, 1000 μm, 2000 μm, and 2000 μm from the foveal center, respectively. Cone analysis maps of the density, spacing, and Voronoi domains are shown with color scales for each of the four areas.
Abbreviation: F, foveal center.

the macula by fundus autofluorescence imaging in patients with retinitis pigmentosa.[2,3,8] In fact, previous studies have reported that an abnormal parafoveal ring of high-density fundus autofluorescence was observed in more than half of patients with retinitis pigmentosa studied.[2,5] The high-density parafoveal fundus autofluorescence ring area represented a transition between the functional and dysfunctional retina, and the diameter and area of the high-density fundus autofluorescence ring were significantly correlated with retinal sensitivity and lengths of the IS/OS line and cone outer segment tips line in patients with retinitis pigmentosa.[2,5,6]

In the present study, we used an adaptive optics fundus camera to observe cone photoreceptors in vivo and showed that the blurred areas of cone mosaics in adaptive optics images corresponded to the high-density fundus autofluorescence ring in the fundus autofluorescence images and

Table 2 Results of cone analyses at four areas in the macula of the right eye in case 2 and healthy control eyes

	T2000	T1000	N1000	N2000
Density (/mm²)				
Case 2	16267	7371	7180	4820
Healthy control (n = 5)	13822 ± 1395	19671 ± 2794	16979 ± 1853	12886 ± 1213
Spacing (μm)				
Case 2	8.67	12.06	12.45	15.06
Healthy control (n = 5)	9.40 ± 0.47	8.10 ± 0.43	8.49 ± 0.46	9.71 ± 0.38
Voronoi (% of six-sided polygons)				
Case 2	40.9	30.8	34.6	34.0
Healthy control (n = 5)	46.0 ± 2.4	51.7 ± 3.6	44.9 ± 2.4	41.9 ± 3.2

Note: Data for healthy controls are shown as the mean ± standard deviation.

to the border of the external limiting membrane and the IS/OS line in OCT images. Because a previous histological study[9] found that the foveal center had high cone densities of 100,000–324,000/mm^2, we concluded that the adaptive optics fundus camera did not have sufficient resolution to distinguish between individual cones at the foveal center. Therefore, cone analyses at the foveal center were not performed. Loss of the external limiting membrane, IS/OS line, and cone outer segment tips line in the OCT images may represent loss of cell bodies of photoreceptors, which appeared as dark patchy areas without cone mosaics or blurred reflections in adaptive optics images in case 1. The area with a detectable external limiting membrane in the OCT images showed decreased cone mosaics and blurred reflections in adaptive optics images as well as relatively normal autofluorescence in fundus autofluorescence images. However, as shown in Tables 1 and 2, the areas outside of the high density fundus autofluorescence ring (T1100 and N1300 in case 1 and T2000 in case 2) showed higher densities than those at the ring (T600 and N600 in case 1 and T1000 in case 2). We compared the results of cone analyses for the five healthy control eyes and two eyes of patients with retinitis pigmentosa using the same manufacturer's software. Although the high-density fundus autofluorescence ring corresponded to the area with low cone densities, the nasal area of case 1 (N1300) and the temporal area of case 2 (T2000) in the region outside of the ring showed relatively normal cone densities that corresponded to the cone density maps in both cases. These results suggest that degeneration of photoreceptors might occur unevenly in retinitis pigmentosa, even though a high-density fundus autofluorescence ring was observed.

Histopathological studies of retinitis pigmentosa have shown that dysfunction of the rods precedes that of the cones and that the shortening of the rod outer segments and photoreceptor cell death occur at the mid-peripheral retina.[1,10] Photoreceptors in all types of retinitis pigmentosa were decreased at the parafoveal areas by up to 1.5 mm compared with normal retinas.[8] After the death of photoreceptors, the retinal pigment epithelium migrates into the inner retina, and the processes of Mueller cells become hypertrophied.[1]

In both of the cases reported here, the cone densities were decreased in a wide area of the temporal and nasal retina. Cone spacing and Voronoi analyses showed similar abnormalities. In the cone density maps of both cases, more cones were observed in nasal areas outside of the ring (N1300 in case 1) and in the temporal area of the parafoveal high-density fundus autofluorescence ring (T2000 in case 2), suggesting that the rate of loss of photoreceptors might be different in the nasal area from that in the temporal area. The patchy dark areas around the fovea in the adaptive optics images may represent a loss of photoreceptors and proliferation of retinal pigment epithelium.

In this study we demonstrated that cone photoreceptors were decreased in the macula of patients with retinitis pigmentosa and especially at the abnormal high-density fundus autofluorescence ring using an adaptive optics fundus camera. The abnormal findings on OCT and fundus autofluorescence images were correlated with the decrease in cone photoreceptors shown by adaptive optics images. The results suggest that adaptive optics images may have advantages for visualizing the horizontal distribution of cone photoreceptors and increasing our understanding of the pathophysiology of retinitis pigmentosa. Further studies using adaptive optics fundus imaging are needed to evaluate successive changes in the cone photoreceptors of patients with retinitis pigmentosa over the long term.

Disclosure

The authors report no conflicts of interest in this work.

References

1. Milam AH, Li ZY, Fariss RN. Histopathology of the human retina in retinitis pigmentosa. *Prog Retin Eye Res*. 1998;17:175–205.
2. Mitamura Y, Mitamura-Aizawa S, Nagasawa T, Katome T, Eguchi H, Naito T. Diagnostic imaging in patients with retinitis pigmentosa. *J Med Invest*. 2012;59:1–11.
3. Wakabayashi T, Sawa M, Gomi F, Tsujikawa M. Correlation of fundus autofluorescence with photoreceptor morphology and functional changes in eyes with retinitis pigmentosa. *Acta Ophthalmol*. 2010;88:177–183.
4. Kellner U, Kellner S, Weber BHF, Fiebig B, Weinitz S, Ruether K. Lipofuscin- and melanin-related fundus autofluorescence visualize different retinal pigment epithelial alterations in patients with retinitis pigmentosa. *Eye*. 2009;23:1349–1359.
5. Murakami T, Akimoto M, Ooto S, et al. Association between abnormal autofluorescence and photoreceptor disorganization in retinitis pigmentosa. *Am J Ophthalmol*. 2008;145:687–694.
6. Aizawa S, Mitamura Y, Hagiwara A, Sugawara T, Yamamoto S. Changes of fundus autofluorescence, photoreceptor inner and outer segment junction line, and visual function in patients with retinitis pigmentosa. *Clin Experiment Ophthalmol*. 2010;38:597–604.
7. Duncan JL, Zhang Y, Gandhi J, et al. High-resolution imaging with adaptive optics in patients with inherited retinal degeneration. *Invest Ophthalmol Vis Sci*. 2007;48:3283–3291.
8. Lenassi E, Troeger E, Wilke R, Hawlina M. Correlation between macular morphology and sensitivity in patients with retinitis pigmentosa and hyperautofluorescent ring. *Invest Ophthalmol Vis Sci*. 2012;53:47–52.
9. Curcio CA, Sloan KR, Kalina RE, Hendrickson AE. Human photoreceptor topography. *J Comp Neurol*. 1990;292:497–523.
10. Stone JL, Barlow WE, Humayun MS, de Juan E Jr, Milam AH. Morphometric analysis of macular photoreceptors and ganglion cells in retinas with retinitis pigmentosa. *Arch Ophthalmol*. 1992;110:1634–1639.